Published in final edited form as:
Am J Physiol Heart Circ Physiol. 2006 March ; 290(3): H978–H984.

Functional and structural remodeling of the myocardial microvasculature in early experimental hypertension

Martin Rodriguez-Porcel[*], **Xiang-Yang Zhu**[†], **Alejandro R. Chade**[†], **Beatriz Amores-Arriaga**[†], **Noel M. Caplice**[*], **Erik L. Ritman**[*,‡], **Amir Lerman**[*], and **Lilach O. Lerman**[†,*]

* *From the Department of Internal Medicine, Divisions of Cardiovascular Diseases and*

† *Nephrology and Hypertension, and the*

‡ *Department of Physiology and Biomedical Engineering, Mayo Clinic College of Medicine, Rochester, MN*

Abstract

Advanced hypertension (HT), associated with left ventricular hypertrophy (LVH), impairs myocardial microvascular function and structure and leads to increased myocardial hypoxia and growth factor activation. However, the effect of HT on microvascular architecture and its relation to microvascular function, prior to the development of LVH (early HT), remain unclear.

Methods—Pigs were studied after 12 weeks of renovascular HT (n=7) or control (n=7). Myocardial microvascular function (blood volume and blood flow at baseline and in response to adenosine) was assessed using electron beam computed-tomography (CT). Microvascular architecture was subsequently studied ex-vivo using micro-CT, and microvessels (diameter<500μm) counted in-situ in 3-D images (40μm on-a-side cubic voxels). Myocardial expression of vascular endothelial growth factor, basic fibroblast growth factor, and hypoxia inducible factor-1α were also measured.

Results—Left ventricular muscle mass was similar between the groups. The blood volume response to intravenous adenosine was attenuated in HT compared to normal animals (+7.4±17.0 vs. +46.2 ±12.3 % compared to baseline, p=0.48 and p=0.01, respectively). Microvascular spatial density in HT was significantly elevated compared to normal (246±26 vs. 125±20 vessels/cm^2, p<0.05) and correlated inversely with the blood volume response to adenosine. Growth factors expression was increased in HT compared to control.

Conclusion—Early HT elicits changes in myocardial microvascular architecture, which are associated with microvascular dysfunction and precede changes in muscle mass. These observations underscore the direct and early effects of HT on the myocardial vasculature.

Keywords

hypertension; microcirculation; imaging; growth factors; micro-CT

Introduction

Hypertension (HT) is a major risk factor for the development and progression of ischemic heart disease, and increases the incidence of cardiac events (13). Advanced HT leads to the development of left ventricular hypertrophy (LVH), which has been associated with abnormal myocardial microvascular function, myocardial architectural changes (9,41), and myocardial ischemia (41,44,45). However, the effect of early HT, prior to the development of LVH, on

Address for correspondence: Lilach O. Lerman, MD, PhD, Division of Nephrology and Hypertension, Mayo Clinic, 200 First Street SW, Rochester, MN 55905. E-Mail: Lerman.Lilach@Mayo.Edu Phone: 507-266-9376 Fax: 507-266-9316.

the myocardial microvasculature (structure and function) are not well understood. We have recently shown that early HT was associated with an impairment in both coronary vascular response to vasodilators (35) *in vitro*, and myocardial perfusion response to cardiac vasodilator challenge *in vivo* (31,33). However, it is yet unknown whether these functional alterations are coupled with changes in myocardial microvascular architecture. Furthermore, the adequacy of such changes in the architecture of myocardial microvessels to sustain their function remains to be elucidated.

Remodeling of the myocardial microvascular architecture, like neovascularization, may represent an adaptive response of the coronary circulation to episodes of myocardial ischemia or sustained pressure overload (37), and is regulated by growth factors and their receptors acting in concert (14). In particular, basic fibroblast growth factor (bFGF) (5,16) and vascular endothelial growth factor (VEGF) (36), regulated through hypoxia inducible factor (HIF)-1α (26), can mediate compensatory neovascularization, as described in the aortic vasa-vasora in advanced HT (18) and in the coronary microvessels during the acute phase of adaptive cardiac hypertrophy (37). However, their role in early HT is yet to be determined.

One of the main factors that restricted investigation of the intra-myocardial microcirculation is the limited availability of accurate and high-resolution imaging methods to study both myocardial microvascular function and 3-D architecture in-situ. We have previously shown that electron beam computed tomography (EBCT) allows accurate and non-invasive assessment of microvascular function *in-vivo*, including myocardial perfusion, microvascular blood volume, and permeability (32,33). In addition, micro Computed Tomography (microCT) is a unique and high-resolution technique that allows investigation of small-scale structures within organs (12). We have previously shown that it permits assessment of the 3D pattern of microvascular structure, spatial distribution, and connectivity (2,3,34,48). The combined application of these two powerful functional imaging techniques may therefore provide a unique insight into the concurrent functional and structural changes of the intramyocardial microcirculation at an early stage of HT, and thereby provide an assessment of the functional impact and adequacy of microvasculature changes that take place in early HT.

Thus, the present study was designed to test the hypothesis that early HT is associated with growth factor activation and changes in myocardial microvascular architecture, such as neovascularization. Furthermore, that the increased spatial density of myocardial microvessels would correlate with the extent of their dysfunction *in vivo* (e.g. the degree of myocardial blood volume response to adenosine).

Materials and Methods

All procedures were approved by the Institutional Animal Care and Use Committee. Female domestic pigs (55–65 kg, 6 months of age) were studied after twelve weeks of observation. Group 1 had no intervention (n=7), while in group 2 renovascular HT (n=7) was induced by placing a local irritant stent in the left renal artery, with consequent renal artery stenosis and development of hypertension (21). After twelve weeks, animals were studied in-vivo and blood samples were collected for measurement of plasma renin activity (PRA). Animals were then euthanized with intravenous pentobarbital (20 cc of Sleepaway®, Fort Dodge Laboratories, Fort Dodge, IA), the heart immediately removed and prepared for microCT, as previously described (34,48). In addition, transmural pieces of the myocardium were flash frozen in liquid nitrogen or preserved in formalin for measurement of growth factor expression.

Left ventricular muscle mass and microvascular function (EBCT)

For in-vivo studies, animals were anesthetized with ketamine and xylazine (20mg/kg and 2 mg/kg, respectively), intubated and mechanically ventilated. Catheters were placed

fluoroscopically in the aorta, for measurement of mean arterial pressure (MAP), and in the right atrium for contrast media injections. Animals were then placed in the EBCT scanning gantry (32,33).

To exclude LVH, LV muscle mass was then measured (33). After allowing 15 minutes for stabilization, end-diastolic tomographic scans (from LV apex to base, slice thickness of 7mm) were acquired using ECG triggering. Scans were obtained during continuous infusion of iopamidol-370 (Squibb, Princeton, NJ, 0.5 cc/kg), which enables distinguishing the endocardial border from the contrast-filled LV cavity during subsequent image analysis. The endocardial and epicardial borders were then manually traced and LV muscle mass calculated as a product of myocardial muscle area, density, and slice thickness, as previously shown (33).

For assessment of myocardial vascular function, scanning was performed in the EBCT flow mode, in which forty consecutive end-diastolic scans were obtained over 40 sec (at 1–3 heart beat intervals) after a 2-sec injection of iopamidol-370 (0.3 cc/kg) into the right atrium. Scans were obtained at baseline and after a 10-minute IV adenosine infusion (400 mcg/min). Intravenous adenosine induces coronary artery vasodilation, and is the most common pharmacological cardiac challenge used to assess myocardial perfusion reserve in clinical practice.

For image analysis, regions of interest were obtained from the LV cavity (for input function) and the anterior cardiac wall. The average tissue density (CT numbers) during and consequent to transit of contrast media was then measured in each region of interest and plotted against time, yielding time-density curves. Each myocardial time-density curve was then stripped into two components, representing the transit of contrast media through the intravascular and extravascular compartments of the myocardium, using extended gamma-variate curve-fitting algorithm (22) (Figure 1). The area enclosed under each curve and its first moment (an index of mean transit time) were then computed (32,33).

Intramyocardial BV was then calculated, using previously validated algorithms (22), as: Intramyocardial BV (mL blood/cc tissue): myocardial tissue area/LV cavity area where ‘area’ is the area under the corresponding curve. Intramyocardial BV, or vascular volume fraction, is a useful index of myocardial microvascular function in response to challenge (20,27). Myocardial perfusion (ml/min/g) was calculated (32,33) as: $60\times(BV/\text{mean transit time})/(1.05\times(1-BV))$, where 1.05 g/cc is the specific density of the myocardium. MBF (ml/min) was subsequently calculated as perfusion × LV muscle mass, and MVR (dyne-sec^{-1} cm^{-5}) as 80*MAP/MBF (33).

Microvascular architecture (MicroCT)

Hearts were prepared as previously described (34,48). The distal left anterior descending artery was cannulated and perfused with a solution of 0.9% normal saline and heparin, and an intravascular contrast agent, radiopaque microfil silicone rubber (MV-122, Flow Tech, Inc, Carver, MA) was perfused through the cannulated LAD at a flow rate of 0.9 ml/min (at a physiological perfusion pressure of 100 ml/min) until it flowed freely from the myocardial veins. To allow for complete relaxation the hearts were kept at 4°C for a day (34), after which a transmural portion of the LV myocardium (approximately 2×1×1 cm^3) was sectioned and prepared for scanning (34,48).

The micro-CT scanner has been previously described (12,34). Myocardial samples were scanned using 0.49º angular increments, providing 721 views around 360º (34). Images were recorded, digitized, and transferred to a controlling computer. The 3D volume images, which consisted of cubic voxels of 20μm on-a-side, were displayed at 40μm on-a-side resolution (to

decrease computer memory demand), and the radiopacity of each voxel was represented by a 16-bit gray-scale value.

Image analysis was performed using the ANALYZE™ software package (Biomedical Imaging Resource, Mayo Clinic, Rochester, MN) (2,34,48). The myocardium was three-dimensionally oriented to obtain anatomically comparable samples for study. Subsequently, the myocardium was divided into two equal parts, classified as subendocardium and subepicardium.

In each region, microvessels (diameters <500μm) were counted in each tomographic section using "Object Counter" software, and classified as either small (diameters between 80 and 200μm) or large (diameters of 201–500μm). In addition, diameters of microvessels larger than 200 μm were manually measured (48). To avoid errors due to noise, microvessels smaller than 80 μm (under two voxels) were excluded and considered to be below resolution.

In addition, using a "connectivity" program, a single intra-myocardial artery and its branches were tomographically isolated in each pig. Their branching pattern was visually assessed in 3D images (34,47,48) and compared between the groups, to evaluate whether a change in microvascular density (quantified in cross-sectional images) was due to an increase in parallel vessels or due to increased branching from existing vessels.

Myocardial Tissue

Expression of HIF-1α (the inducible subunit of HIF-1) mRNA was measured by real time RT-PCR. Protein expression of HIF-1α and VEGF were detected by Western blotting (48), while levels of bFGF were investigated using ELISA (Quantikine, R&D Systems, Minneapolis, MN). For localization of FGF and VEGF, immunohistochemistry was used as previously described (4,48). Mouse monoclonal antibodies anti-VEGF (A-20, dilution 1:100, R&D Systems, Minneapolis, MN) and bFGF-2 (#147, 1:100, R&D Systems, Minneapolis, MN) served as primary antibodies.

Western Blotting

Equal protein (50 to 100 μg) of myocardial homogenate was dissolved in sodium dodecyl sulfate–polyacrylamide gels (12% or 4% to 20%) under reducing conditions and electrophoretically transferred onto polyvinylidene difluoride membranes (Bio-Rad, Hercules, CA). Membranes were blocked for 1 hour in TBST/5% nonfat milk and incubated overnight at 4°C with antibodies against HIF-1α (1:1000 Novus Biologicals, Littleton, CO) or VEGF (1:200, Santa Cruz Biotechnology, Santa Cruz, CA), as previously described from our laboratory (3,48). After being washed with TBST, the membranes were incubated for 1 hour with horseradish peroxidase–linked anti-rabbit antibody (1:5000, Amersham Pharmacia Biotech, Piscataway, NJ) in TBST/5% milk, and proteins were visualized by electrochemiluminescence. α-Actin (1:1000, Sigma, St. Louis, MO) was used as the loading control (47,48).

Real Time RT- PCR

Total RNA was isolated from myocardial tissue with the TRIZOL (Invitrogen, Carlsbad, CA) method. cDNA was synthesized with the Invitrogen Superscript first-strand synthesis kit, as we have previously described (47,48).

To measure the expression of HIF-1α mRNA, real time quantitative RT-PCR was subsequently performed with a SYBR Green jumpstart Taq ReadyMix kit (Sigma, St. Louis, MO). The porcine gene-specific sequence of HIF-1α was (left) 5′-AAC AAT TCA TCT GCG CCT TC-3′ and (right) 5′-AAC AAT TCA TCT GCG CCT TC-3′. The relative amount of HIF-1α mRNA was normalized to an internal control glycerylaldehyde 3-phospate dehydrogenase (GADPH)

and relative to a calibrator (normal), calculated by $2^{-\Delta\Delta CT}$. The sequence of the GADPH primer was (upper) 5′-GTC CAT GAA CCA TGA GAA GT-3′ and (lower) 5′-GTC TTC TGG GTG GCA GTG AT-3′ (47,48).

Statistical Analysis

Data are mean±SEM. Comparisons were performed using unpaired or paired Student's t-test (between and within groups, respectively). Statistical significance was accepted for $p \leq 0.05$. Correlation analysis was performed by least-squares linear regression using the StatView 5.1 statistical software package (SAS Institute Inc, Cary, NC.)

Results

In hypertensive animals, MAP was significantly increased compared to normal (Table 1), while PRA and LV muscle mass were not significantly different between the groups (Table 1).

Myocardial vascular architecture

The transmural spatial density of microvessels was significantly increased in HT animals compared to normal (246±26 vs. 125±20 vessels/cm^2, p=0.02). This resulted from increased spatial density in both the subepicardium and subendocardium (Figure 2, Table 1), but was significantly more pronounced in the subendocardial region (Figure 2, Table 1). In both regions, increases in microvascular density appeared to be secondary to increased branching of small microvessels, as they were tomographically connected to the main vessel (Figure 2, bottom). The microvascular density of large microvessels was also slightly but significantly increased in both sub-regions (Table 1), while their mean diameter was significantly reduced ($p<0.01$, Table 1).

Myocardial vascular function

Baseline BV, MBF, and MVR were not significantly different between normal and HT animals (Table 1). Matched datasets of functional responses and vessel density were available in 7 HT and 5 control animals. Compared to normal animals, the increase in BV and MBF in response to intravenous adenosine was blunted in HT and was not significantly different from baseline (Figure 3, top). MVR significantly decreased in response to adenosine in normal animals, but this decrease was blunted in HT (−27.7± 5.8 vs. −11.4±11.8% compared to baseline, p=0.02 and p=0.16, respectively).

Interestingly, HT animals that showed the greatest increase in vessel density also showed the most attenuated BV response to adenosine. Furthermore, this relationship disclosed a significant inverse correlation between the spatial density of myocardial microvessels and the functional BV responses to adenosine in the anterior wall of HT animals (r=−0.75, p=0.04, Figure 3, bottom right), but not in normal animals (r=0.01, p=0.85, Figure 3, bottom left).

Ex-vivo studies

HT animals showed increased HIF-1α protein expression compared to controls (Figure 4), with a tendency for an elevation of mRNA levels. Myocardial levels and expression of bFGF (in vascular smooth muscle cells and myocytes) and VEGF (in endothelial cells) were significantly increased in HT animals compared to normal, and distributed uniformly throughout the myocardium (Figure 5).

Discussion

This study demonstrates that experimental HT induces changes in myocardial microvascular architecture and function in association with activation of growth factors, which precede the development of LVH.

HT is a major risk factor and leads to increased incidence of cardiovascular events (1,25). HT is characterized by coronary endothelial dysfunction (42), abnormal myocardial perfusion regulation (10), and changes in myocardial microvascular architecture (9,41). However, many of these changes were characterized in established or advanced stages of the disease, such as in the presence of LVH (9,41). Thus, it has been difficult to discern the effects of HT *per se* on the myocardium from the effects of LVH. We have previously shown that in a model of swine renovascular hypertension, moderate increases in blood pressure for a relatively short period of time were not necessarily associated with increases in LV muscle mass (33,35). Using this swine model of early HT, we have previously demonstrated that coronary endothelial dysfunction (35) and abnormal myocardial perfusion response to cardiac challenge (33) in early HT occur independently and prior to the development of LVH. The current study extends these prior observations and demonstrates that similar to microvascular dysfunction (represented in abnormal BV response to cardiac challenge), myocardial architectural changes in HT are initiated in the early stages of the disease and precede an increase in LV muscle mass, implying a direct effect of HT on both myocardial architecture and function.

To visualize and quantify the 3D architecture of the myocardial microvasculature, we employed a unique, high-resolution microCT technique, which enabled detection of vessel size-specific alterations (2,34,48). We have previously described the capability of microCT to detect changes in myocardial and renal microvascular architecture in diet-induced hypercholesterolemia and ischemia (34,47). Due to its high-resolution and image analysis capabilities, this technology permits the evaluation of organ microvasculature, its distribution pattern and connectivity (34,47). Using this technique, we observed that the HT-induced neovascularization was mainly due to an increase in the number of microvessels <200μm in diameter, which are largely responsible for myocardial vascular resistance, and was more pronounced in the subendocardial myocardium. Indeed, the subendocardial architectural changes observed in our study likely reflect the differential sensitivity of sub-endocardial microvessels to nitric oxide and superoxide anion (39) or the increased propensity of this region for ischemia (28).

The abnormal myocardial microvascular function seen in HT may be associated with episodes of myocardial ischemia (11), and thereby upregulate the expression of HIF-1α (23). In addition, abnormal coronary endothelial function in early HT (35) likely contributes to tissue ischemia and increased hypoxia. These ischemic stimuli can subsequently trigger myocardial neovascularization by modulating the temporal and spatial expression and activity of a plethora of growth factors and their receptors, which may play different roles in special aspects of vessel formation (24).

VEGF and bFGF are two key angiogenic factors that have been associated with HT (16,46) and can be induced in pathophysiological states like chronic hypoxia (15,48). This study extends prior observations and shows that a short duration of experimental HT is sufficient to induce significant myocardial ischemia in conjunction with VEGF and bFGF activation. These data are in agreement with prior studies that have shown that hypoxia serves as a powerful stimulus for the activation of VEGF (48) and bFGF (17,43). In addition, myocardial neovascularization observed in our study could have also resulted from the synergistic interaction of VEGF and bFGF with alternative pathways, such as the local renin-angiotensin-system (29) or other angiogenic factors.

In addition, we observed that HT was associated with a decrease in mean diameter of large microvessels, possibly due to inward growth of the vascular wall (negative vascular remodeling). Both the expression of angiogenic factors (16) and sensitivity to their growth stimulatory actions (6) may be enhanced in HT, which may contribute to vascular wall thickening (33). The increased number of small microvessels in the face of decreased diameter of large microvessels might have been responsible for maintaining basal microvascular blood volume and MBF unaltered, as previously observed in asymptomatic patients with borderline hypertension and no LVH (19). A slight (albeit not significant) increase in MBF that paralleled the increase in MAP likely sustained MVR.

The powerful combination of anatomical assessment using microCT with functional assessment of myocardial vascular function using EBCT allowed exploration of the relation between microvascular anatomy and function, which becomes critically important in view of the growing interest in therapeutic interventions targeted to increase the number of vessels (38), with the ultimate goal of improving organ function. Interestingly, we observed that microvascular neovascularization was inversely related to myocardial BV response to challenge in early HT, implying that an increase in the number of vessels did not translate into an improvement of myocardial function, but on the contrary was associated with worsening of the myocardial functional response. This may be due to abnormal features like disorganized architecture (8) and functional abnormalities (7) that can characterize newly generated microvessels, and which may lead to altered regulation of flow to the myocardium. Nevertheless, because pathologic neovascularization (like in HT) may have different mechanisms and effects than therapeutic neovascularization, these results should not be extrapolated to states where therapeutic angiogenesis might be beneficial.

Limitations

In the current study we describe the microvascular changes that occur in early hypertension, mostly in vessels under 200 μm in diameter. Although the resolution of micro-CT is as high as 4 μm voxels, limited computing power currently restricts routine handling of such large image files. In the current study we used 40 μm voxels, and enhancement of less than two adjacent voxels was considered noise, so that analysis was restricted to myocardial microvessels 80 μm or larger. Rapid progress in memory size and computing power will likely allow future analysis of much smaller vessels.

It is also possible that microvessels might have been misclassified due to vascular remodeling or residual vascular tone with a consequent decline in the diameter of large microvessels. However, this is unlikely because our tissue preparation allows for full vascular relaxation, and the number of large microvessels was in fact increased rather than decreased.

In this study we used relatively young pigs, which may show greater potential for angiogenic responses compared to older subjects (30). Notably, we also used female pigs, and estrogen has been reported to increase angiogenic response in HT (40). However, the pigs in our experimental groups were pre-menstrual, so that hormonal changes were unlikely to interfere with our results. Nevertheless, the possibility of age and gender effects cannot be ruled out.

In summary, this study demonstrates that myocardial microvascular changes in early HT are associated with hypoxia and growth factor activation, as well as with microvascular functional changes. Importantly, we have shown that architecture changes in the myocardial microcirculation precede development of LVH, and that an increase in its density did not translate into improved myocardial microvascular function in HT. These observations support the notion that early hypertension has direct functional and structural effects on the myocardial microcirculation. These findings have clinical implications, as these changes occur after a relatively short period of moderate HT. These results underscore the functional significance

of the architectural changes present in early HT and support early application of intensive preventive and therapeutic strategies in patients with HT.

Acknowledgements

This study was supported by NIH grants HL63282, HL77131, HL65342, and EB 000305, and by the AHA.

References

1. Aronow WS, Epstein S, Koenigsberg M. Usefulness of echocardiographic left ventricular hypertrophy and silent ischemia in predicting new cardiac events in elderly patients with systemic hypertension or coronary artery disease. Angiology 1990;41:189–193. [PubMed: 2137998]
2. Bentley MD, Rodriguez-Porcel M, Lerman A, Sarafov MH, Romero JC, Pelaez LI, Grande JP, Ritman EL, Lerman LO. Enhanced renal cortical vascularization in experimental hypercholesterolemia. Kidney Int 2002;61:1056–1063. [PubMed: 11849461]
3. Chade AR, Bentley MD, Zhu X, Rodriguez-Porcel M, Niemeyer S, Amores-Arriaga B, Napoli C, Ritman EL, Lerman A, Lerman LO. Antioxidant intervention prevents renal neovascularization in hypercholesterolemic pigs. J Am Soc Nephrol 2004;15:1816–1825. [PubMed: 15213269]
4. Chade AR, Rodriguez-Porcel M, Grande JP, Krier JD, Lerman A, Romero JC, Napoli C, Lerman LO. Distinct renal injury in early atherosclerosis and renovascular disease. Circulation 2002;106:1165–1171. [PubMed: 12196346]
5. Cottone S, Vadala A, Vella MC, Nardi E, Mule G, Contorno A, Riccobene R, Cerasola G. Changes of plasma endothelin and growth factor levels, and of left ventricular mass, after chronic AT1-receptor blockade in human hypertension. Am J Hypertens 1998;11:548–553. [PubMed: 9633790]
6. Damon DH, Lange DL, Hattler BG. In vitro and in vivo vascular actions of basic fibroblast growth factor (bFGF) in normotensive and spontaneously hypertensive rats. J Cardiovasc Pharmacol 1997;30:278–284. [PubMed: 9300309]
7. Dvorak HF, Brown LF, Detmar M, Dvorak AM. Vascular permeability factor/vascular endothelial growth factor, microvascular hyperpermeability, and angiogenesis. Am J Pathol 1995;146:1029–1039. [PubMed: 7538264]
8. Gerwins P, Skoldenberg E, Claesson-Welsh L. Function of fibroblast growth factors and vascular endothelial growth factors and their receptors in angiogenesis. Crit Rev Oncol Hematol 2000;34:185–194. [PubMed: 10838264]
9. Gu JW, Fortepiani LA, Reckelhoff JF, Adair TH, Wang J, Hall JE. Increased expression of vascular endothelial growth factor and capillary density in hearts of spontaneously hypertensive rats. Microcirculation 2004;11:689–697. [PubMed: 15726836]
10. Harrison DG, Florentine MS, Brooks LA, Cooper SM, Marcus ML. The effect of hypertension and left ventricular hypertrophy on the lower range of coronary autoregulation. Circulation 1988;77:1108–1115. [PubMed: 2966018]
11. Hasdai D, Gibbons RJ, Holmes DR Jr, Higano ST, Lerman A. Coronary endothelial dysfunction in humans is associated with myocardial perfusion defects. Circulation 1997;96:3390–3395. [PubMed: 9396432]
12. Jorgensen SM, Demirkaya O, Ritman EL. Three-dimensional imaging of vasculature and parenchyma in intact rodent organs with X-ray micro-CT. Am J Physiol 1998;275:H1103–1114. [PubMed: 9724319]
13. Kannel WB. Historic perspectives on the relative contributions of diastolic and systolic blood pressure elevation to cardiovascular risk profile. Am Heart J 1999;138:205–210. [PubMed: 10467214]
14. Kersten JR, Pagel PS, Chilian WM, Warltier DC. Multifactorial basis for coronary collateralization: a complex adaptive response to ischemia. Cardiovasc Res 1999;43:44–57. [PubMed: 10536689]
15. Kosmidou I, Xagorari A, Roussos C, Papapetropoulos A. Reactive oxygen species stimulate VEGF production from C(2)C(12) skeletal myotubes through a PI3K/Akt pathway. Am J Physiol Lung Cell Mol Physiol 2001;280:L585–592. [PubMed: 11237996]
16. Kurz C, Hefler L, Zeisler H, Schatten C, Husslein P, Tempfer C. Maternal basic fibroblast growth factor serum levels are associated with pregnancy-induced hypertension. J Soc Gynecol Investig 2001;8:24–26.

17. Kuwabara K, Ogawa S, Matsumoto M, Koga S, Clauss M, Pinsky DJ, Lyn P, Leavy J, Witte L, Joseph-Silverstein J, et al. Hypoxia-mediated induction of acidic/basic fibroblast growth factor and platelet-derived growth factor in mononuclear phagocytes stimulates growth of hypoxic endothelial cells. Proc Natl Acad Sci U S A 1995;92:4606–4610. [PubMed: 7538678]
18. Kuwahara F, Kai H, Tokuda K, Shibata R, Kusaba K, Tahara N, Niiyama H, Nagata T, Imaizumi T. Hypoxia-inducible factor-1alpha/vascular endothelial growth factor pathway for adventitial vasa vasorum formation in hypertensive rat aorta. Hypertension 2002;39:46–50. [PubMed: 11799077]
19. Laine H, Raitakari OT, Niinikoski H, Pitkanen OP, Iida H, Viikari J, Nuutila P, Knuuti J. Early impairment of coronary flow reserve in young men with borderline hypertension. J Am Coll Cardiol 1998;32:147–153. [PubMed: 9669263]
20. Le DE, Bin JP, Coggins MP, Wei K, Lindner JR, Kaul S. Relation between myocardial oxygen consumption and myocardial blood volume: a study using myocardial contrast echocardiography. J Am Soc Echocardiogr 2002;15:857–863. [PubMed: 12221400]
21. Lerman LO, Schwartz RS, Grande JP, Sheddy PFII, Romero JC. Non-invasive evaluation of a novel swine model of renal artery stenosis. J Am Soc Neprol 1999;10:1455–1465.
22. Lerman LO, Siripornpitak S, Maffei NL, Sheedy PFII, Ritman EL. Measurement of in vivo myocardial microcirculatory function with electron beam CT. J Comput Assist Tomogr 1999;23:390–398. [PubMed: 10348445]
23. Li QF, Dai AG. Hypoxia-inducible factor-1 alpha regulates the role of vascular endothelial growth factor on pulmonary arteries of rats with hypoxia-induced pulmonary hypertension. Chin Med J (Engl) 2004;117:1023–1028. [PubMed: 15265376]
24. **Matsumoto T and Claesson-Welsh L.** VEGF receptor signal transduction. *Sci STKE* 2001: RE21, 2001.
25. Mehler PS, Coll JR, Estacio R, Esler A, Schrier RW, Hiatt WR. Intensive blood pressure control reduces the risk of cardiovascular events in patients with peripheral arterial disease and type 2 diabetes. Circulation 2003;107:753–756. [PubMed: 12578880]
26. Michiels C, De Leener F, Arnould T, Dieu M, Remacle J. Hypoxia stimulates human endothelial cells to release smooth muscle cell mitogens: role of prostaglandins and bFGF. Exp Cell Res 1994;213:43–54. [PubMed: 8020605]
27. Möhlenkamp S, Lerman LO, Lerman A, Behrenbeck TR, Katusic Z, Sheedy PFII, Ritman EL. Minimally invasive evaluation of coronary microvascular function by electron beam computed tomography. Circulation 2000;102:2411–2416. [PubMed: 11067797]
28. Panting JR, Gatehouse PD, Yang GZ, Grothues F, Firmin DN, Collins P, Pennell DJ. Abnormal subendocardial perfusion in cardiac syndrome X detected by cardiovascular magnetic resonance imaging. N Engl J Med 2002;346:1948–1953. [PubMed: 12075055]
29. Peifley KA, Winkles JA. Angiotensin II and endothelin-1 increase fibroblast growth factor-2 mRNA expression in vascular smooth muscle cells. Biochem Biophys Res Commun 1998;242:202–208. [PubMed: 9439636]
30. Rakusan K, Flanagan MF, Geva T, Southern J, Van Praagh R. Morphometry of human coronary capillaries during normal growth and the effect of age in left ventricular pressure-overload hypertrophy. Circulation 1992;86:38–46. [PubMed: 1535573]
31. Rodriguez-Porcel M, Herrman J, Chade AR, Krier JD, Breen JF, Lerman A, Lerman LO. Long-term antioxidant intervention improves myocardial microvascular function in experimental hypertension. Hypertension 2004;43:493–498. [PubMed: 14718362]
32. Rodriguez-Porcel M, Lerman A, Best PJ, Krier JD, Napoli C, Lerman LO. Hypercholesterolemia impairs myocardial perfusion and permeability: role of oxidative stress and endogenous scavenging activity. J Am Coll Cardiol 2001;37:806–815.
33. Rodriguez-Porcel M, Lerman A, Herrmann J, Schwartz RS, Sawamura T, Condorelli M, Napoli C, Lerman LO. Hypertension exacerbates the effect of hypercholesterolemia on the myocardial microvasculature. Cardiovasc Res 2003;58:213–221. [PubMed: 12667964]
34. Rodriguez-Porcel M, Lerman A, Ritman EL, Wilson SW, Best PJM, Lerman LO. Altered microvascular structure in experimental hypercholesterolemia. Circulation 2000;102:2028–2030. [PubMed: 11044415]

35. Rodriguez-Porcel M, Lerman LO, Herrmann J, Sawamura T, Napoli C, Lerman A. Hypercholesterolemia and Hypertension Have Synergistic Deleterious Effects on Coronary Endothelial Function. Arterioscler Thromb Vasc Biol 2003;23:885–891. [PubMed: 12663373]
36. Shibuya M. Structure and function of VEGF/VEGF-receptor system involved in angiogenesis. Cell Struct Funct 2001;26:25–35. [PubMed: 11345501]
37. Shiojima I, Sato K, Izumiya Y, Schiekofer S, Ito M, Liao R, Colucci WS, Walsh K. Disruption of coordinated cardiac hypertrophy and angiogenesis contributes to the transition to heart failure. J Clin Invest 2005;115:2108–2118. [PubMed: 16075055]
38. Sim EK, Zhang L, Shim WS, Lim YL, Ge R. Therapeutic angiogenesis for coronary artery disease. J Card Surg 2002;17:350–354. [PubMed: 12546086]
39. Sorop O, Spaan JA, Sweeney TE, VanBavel E. Effect of steady versus oscillating flow in porcine coronary arterioles. Involvement of NO and superoxide anion. Circ Res 2003;22:1344–1351. [PubMed: 12764025]
40. Stier CT Jr, Chander PN, Rosenfeld L, Powers CA. Estrogen promotes microvascular pathology in female stroke-prone spontaneously hypertensive rats. Am J Physiol Endocrinol Metab 2003;285:E232–239. [PubMed: 12670833]
41. Tomanek RJ, Palmer PJ, Peiffer GL, Schreiber KL, Eastham CL, Marcus ML. Morphometry of canine coronary arteries, arterioles, and capillaries during hypertension and left ventricular hypertrophy. Circ Res 1986;58:38–46. [PubMed: 2935323]
42. Treasure CB, Klein JL, Vita JA, Manoukian SV, Renwick GH, Selwyn AP, Ganz P, Alexander RW. Hypertension and left ventricular hypertrophy are associated with impaired endothelium-mediated relaxation in human coronary resistance vessels. Circulation 1993;87:86–93. [PubMed: 8419028]
43. Wang L, Xiong M, Che D, Liu S, Hao C, Zheng X. The effect of hypoxia on expression of basic fibroblast growth factor in pulmonary vascular pericytes. J Tongji Med Univ 2000;20:265–267. [PubMed: 12840907]
44. Yamani MH, Massie BM. Hypertension, myocardial ischemia, and sudden death. Curr Opin Cardiol 1994;9:542–550. [PubMed: 7987033]
45. Yurenev AP, DeQuattro V, Dubov PB, Ostroumov EN, Nikulin IA, Konyaeva EB, Balyakina EV, Atachanov SE, Kosenko AI, Popov EG, et al. Silent myocardial ischemia in patients with essential hypertension. Am J Hypertens 1992;5:169S–174S. [PubMed: 1632937]
46. Zacharieva S, Atanassova I, Orbetzova M, Kirilov G, Nachev E, Kalinov K, Shigarminova R. Vascular endothelial growth factor (VEGF), prostaglandin E2(PGE2) and active renin in hypertension of adrenal origin. J Endocrinol Invest 2004;27:742–746. [PubMed: 15636427]
47. Zhu XY, Chade AR, Rodriguez-Porcel M, Bentley MD, Ritman EL, Lerman A, Lerman LO. Cortical microvascular remodeling in the stenotic kidney: role of increased oxidative stress. Arterioscler Thromb Vasc Biol 2004;24:1854–1859. [PubMed: 15308558]
48. Zhu XY, Rodriguez-Porcel M, Bentley MD, Chade AR, Sica V, Napoli C, Caplice N, Ritman EL, Lerman A, Lerman LO. Antioxidant intervention attenuates myocardial neovascularization in hypercholesterolemia. Circulation 2004;109:2109–2115. [PubMed: 15051643]

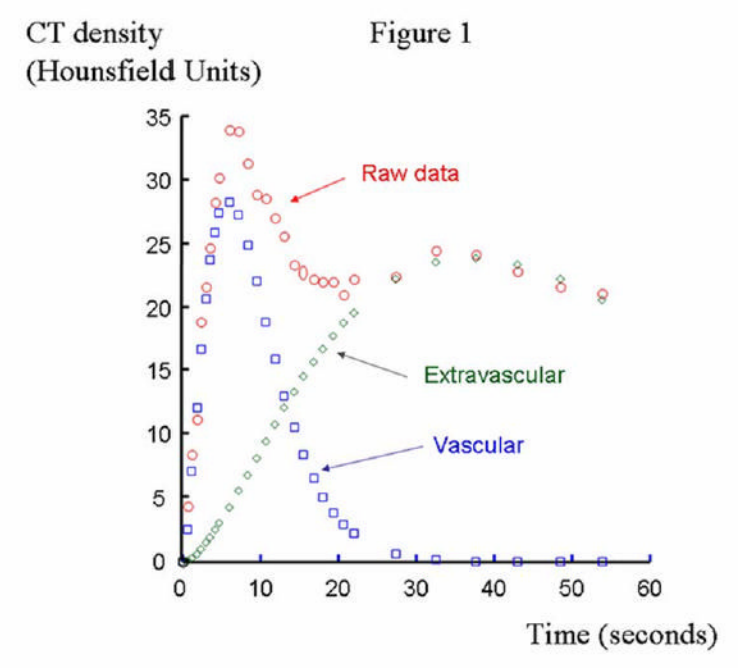

Figure 1.
Time-density curves consequent to transit of contrast media through the anterior cardiac wall region of interest (raw data, red circles). The intra- and extra-vascular components of the original curve were depicted using extended gamma-variate curve-fitting algorithms (intravascular: blue squares and extravascular: green diamonds).

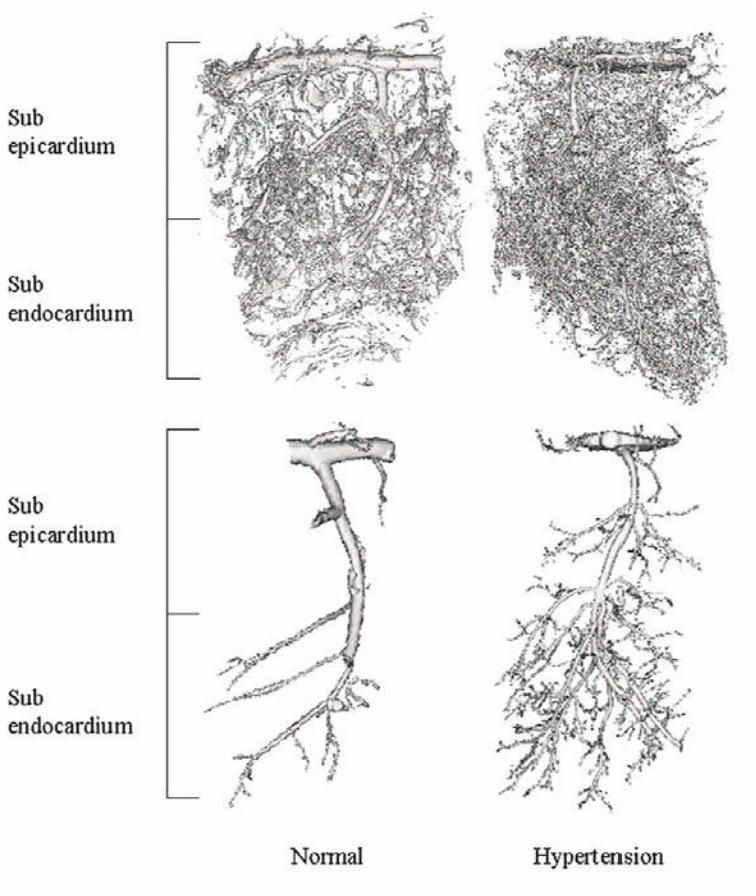

Figure 2.

Top: Representative 3D images of the transmural myocardium in normal and hypertensive (HT) pigs. The samples were scanned with micro computed tomography (microCT), reconstructed at a resolution of 20μm on-a-side cubic voxels, and displayed at 40μm on-a-side spatial resolution. Bottom: Representative 3D images of tomographically isolated intramyocardial coronary arteries (displayed at 20μm on-a-side resolution) of normal and HT pigs.

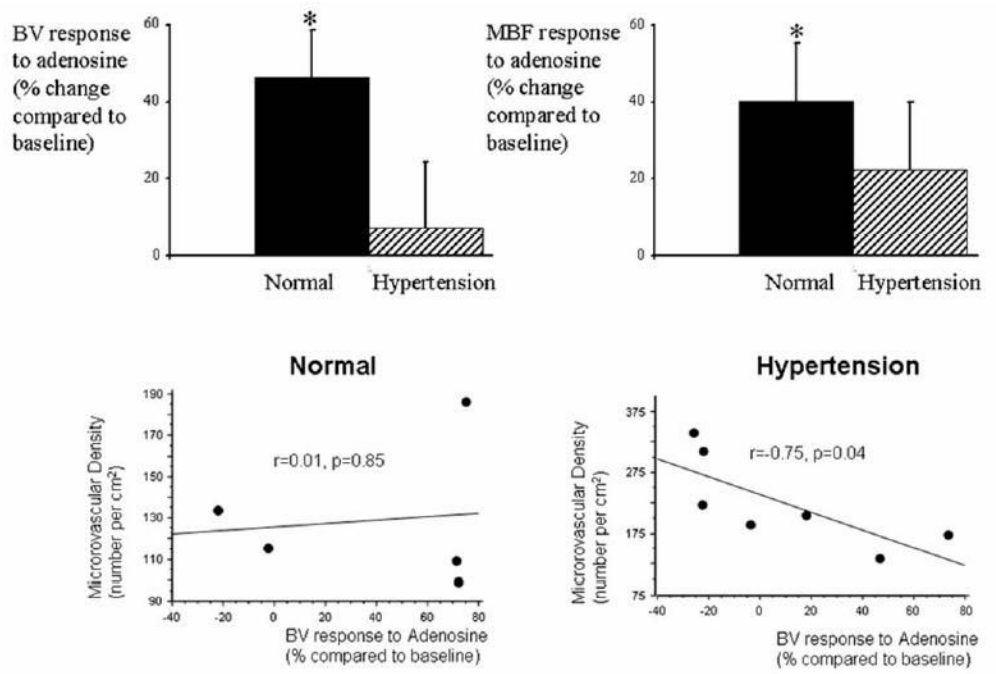

Figure 3.

Top, Electron-beam computed tomography (EBCT)-derived myocardial blood volume (BV, left) and myocardial blood flow (MBF, right) responses to adenosine in (% change compared to baseline) in normal (n=5) and HT (n=7) animals. * $p<0.05$ compared to baseline. Bottom, Correlation between microCT-measured microvascular density and EBCT-derived BV response to adenosine in the anterior wall of control (left) and HT (right), showing that in HT, but not in control, there was significant inverse correlation between microvascular structure and function.

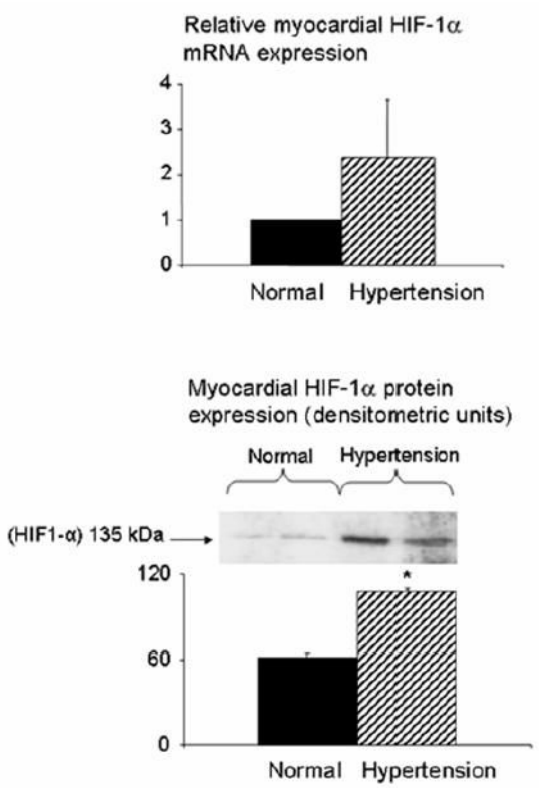

Figure 4.
Expression of HIF-1α mRNA (top) and protein (bottom) in normal and HT pigs. *p<0.05 compared to normal.

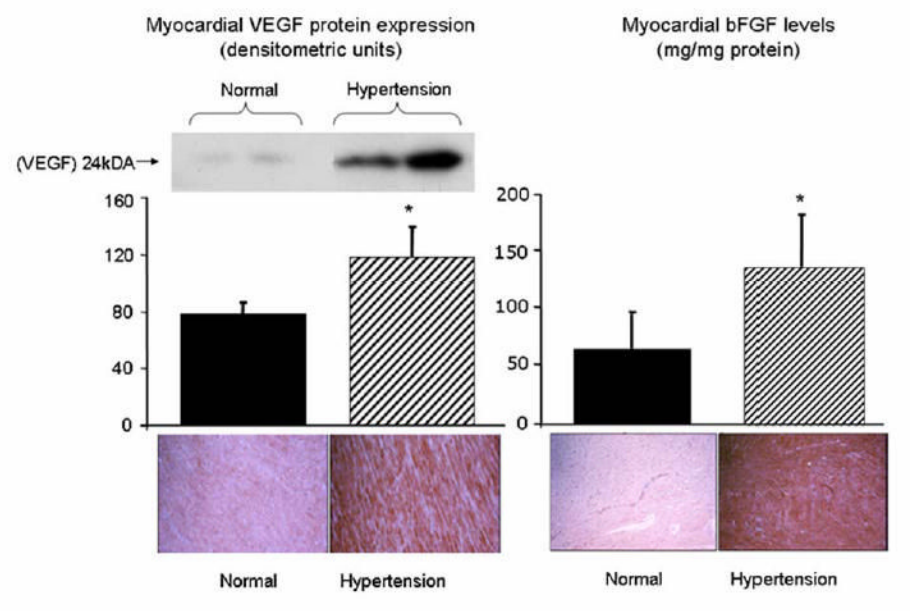

Figure 5.

Left, protein expression of VEGF (Western blot and immunohistochemistry) in the transmural myocardium of normal and HT pigs. Right, level (ELISA) and immunohistochemistry of bFGF in the transmural myocardium of normal and hypertensive pigs. Myocardial expression of both bFGF and VEGF was significantly increased in HT animals. Immunohistochemistry showed that bFGF is expressed mainly in vascular smooth muscle cells and myocytes, and VEGF in endothelial cells, and that their increased expression appears to be uniform throughout the myocardium. *$p<0.05$ compared to normal.

Table 1

Top, baseline characteristics of normal (n=7) and hypertensive (HT, n=7) pigs. Middle, spatial density of small (80–200μm) and large (201–500μm in diameter) microvessels (per cm^2) and mean diameter of large intramyocardial microvessels measured using micro computed tomography in normal and HT pigs. Bottom, EBCT-derived baseline characteristics of normal and HT pigs.

		Normal	HT
Baseline characteristics			
	Mean arterial pressure (mmHg)	102.2±3.9	121.0±8.8*
	Plasma renin activity (pg/ml)	0.4±0.1	0.3±0.1
	Left ventricular muscle mass (grams)	118.3±5.8	122.9±4.4
Microvessels (number per cm^2)			
Subepicardium	Small (81–200 μm)	117±17	176±28*
	Large (201–500 μm)	5.2±1.0	9.3±1.4*
Subendocardium	Small (81–200 μm)	120±12	285±30*†
	Large (201–500 μm)	5.9±1.2	9.8±1.7*
Mean diameter of large microvessels (μm)		282±9	253±8*
EBCT-derived baseline characteristics			
	Myocardial blood volume (mL g^{-1})	0.14±0.04	0.14±0.01
	Myocardial blood flow (mL/min)	99.5±9.2	108.1±19.1
	Myocardial vascular resistance (dyne-sec^{-1} cm^{-5})	91.2±7.9	90.3±14.0

EBCT: electron beam computed tomography.

* $p<0.05$ vs. normal,

† $p<0.01$ compared to the subendocardium of HT.